

Efficient Microcanonical Histogram Analysis and Application to Peptide Aggregation

Michael Bachmann*

*Soft Matter Systems Research Group, Center for Simulation Physics,
Department of Physics and Astronomy, The University of Georgia, Athens, GA 30602, USA*

A novel approach designed to directly estimate microcanonical quantities from energy histograms is proposed, which enables the immediate systematic identification and classification of phase transitions in physical systems of any size by means of the recently introduced generalized microcanonical inflection-point analysis method. The application to the aggregation problem of GNNQQNY heptapeptides, for which the entire transition sequence is revealed, shows the power of this promising method.

In recent decades, computer simulations have become the inevitable tool for systematically approaching a better understanding of the physical behavior of complex systems. Statistical physics has provided the basis for the analysis of the vast amount of data generated in simulations of advanced models ever more precisely accommodating details of the physical systems. The development of efficient simulation techniques has kept pace with the demand by science and technology and the consistently increasing computational resources.

For the important questions aiming at the cooperative behavior of microscopic agents such as atoms or molecules forming stable macroscopic phases, Monte Carlo and thermostated molecular dynamics simulation methods have proven to be particularly useful. Among the most widely used are generalized-ensemble Monte Carlo sampling methods such as parallel tempering [1–4], simulated tempering [5, 6], multicanonical sampling [7–11], and the Wang-Landau method [12, 13]. These techniques were developed to address arguably the most difficult structure formation processes in many-body systems, including spin glasses and protein folding. The latter is a particularly interesting example, because by their very nature, proteins are finite systems on mesoscopic scale, yet exhibiting strong features of cooperativity known from phase transitions in macroscopic systems. Integrating finite, mesoscopic systems into the theory of phase transitions is a vital research problem.

The method proposed here can be readily employed to any set of energy histograms or energy probability distributions. The most obvious application is the combination of the individual histograms obtained in computer simulations at multiple temperatures, although reweighted histograms from generalized-ensemble simulations can also be used, provided additional weights such as multicanonical weight functions artificially introduced to enhance the simulation performance are divided out.

For the following description of the method, we assume a set of I canonical energy histograms $h_i(E)$, $i = 1, 2, \dots, I$ is available. These histograms are the typical outcomes of parallel-tempering Monte Carlo simulations, where I Metropolis Monte Carlo simulations run in parallel threads i . Exchanging replicas between the threads

supports the decorrelation of data and, therefore, improves performance and data quality. This is particularly relevant in simulations across phase transition regions.

The canonical energy histogram obtained in the i th simulation thread at the canonical temperature T_i^{can} is related to the probability density distribution $p_i(E)$ at T_i^{can} :

$$h_i(E) \sim p_i(E) = \frac{1}{Z(T_i^{\text{can}})} g(E) e^{-E/k_B T_i^{\text{can}}}, \quad (1)$$

where $g(E)$ is the density of states, $Z(T_i^{\text{can}})$ the canonical partition function at T_i^{can} , and k_B the Boltzmann factor. As an absolute quantity, Z is not accessible in typical importance-sampling Monte Carlo methods, but usually not of major interest anyway. The key quantity is the density of states as it is not only used for calculations of energetic averages and response quantities such as the specific heat, but it allows for the introduction of the microcanonical entropy

$$S(E) = k_B \ln g(E). \quad (2)$$

This is vital for the recently introduced generalized microcanonical inflection-point analysis method for the systematic identification and classification of phase transitions in physical systems of any size [14], which has found traction in different fields of physics [15–20].

If the simulation was capable of covering the entire energy region of interest, an estimate of the density of states could be directly obtained from the histogram by dividing out the Boltzmann factor. Methods like parallel tempering that can easily be parallelized usually only provide fragmented information, though.

Before discussing the reweighting method and microcanonical analysis from histogram data, a first look at results from actual parallel tempering simulations may be helpful. Figure 1(a) shows the canonical energy histograms obtained in simulations of four identical heptapeptide chains at twelve different temperatures in the range $T_i^{\text{can}} \in [200\text{K}, 500\text{K}]$ ($i = 1, \dots, 12$). The amino acid sequence of an individual chain is GNNQQNY. For these simulations, the internally developed Monte Carlo simulation package for proteins BONSAI (bio-organic nucleation and self-assembly at interfaces) was employed.

The protein model used for the simulations is based on an all-atom, implicit-solvent representation [21, 22]. Each histogram contains the statistics of 10^8 Monte Carlo sweeps, where a sweep is a sequence of updates including torsional rotations about dihedral angles of individual amino acids and rigid-body rotations and translations of entire chains.

The aggregation properties of GNNQQNY, which is a polar segment of the yeast protein Sup35, have been subject to numerous studies [23–26]. Individual chains have the tendency to form β -strands that can nucleate with other chains. Accumulating sufficient statistics for a detailed microcanonical analysis of the nucleation transition that lends insight into the aggregation mechanism across the energy region covering the entire transition sequence is virtually impossible. This can already be seen in Fig. 1(b), where the individual estimates for the microcanonical entropy, obtained by simply dividing out the Boltzmann factor in the histograms, are plotted. Since the tails of those curves are hampered by low statistics in the histograms, the data quality significantly varies, even for a single fragment.

In order to obtain a reliable estimate for the microcanonical entropy (or the density of states), it is necessary to combine these fragmented estimators. This is not straightforward, because an absolute reference point is missing; the partition function cannot be estimated absolutely in these simulations as mentioned above. In fact, the relative shifts between the fragments shown in Fig. 1(b) are not artificial. These are the actual numerical results based on the histogram data.

For an efficient estimation of the density of states, the multi-histogram reweighting method [27, 28] was already introduced decades ago. In this method, error weights are introduced to account for the low statistics in the tails of the canonical histograms. The error-weighted combination of histograms leads to a system of two equations that needs to be solved recursively. The result is an estimate for the density of states, which usually is then used in a subsequent canonical analysis, i.e., calculations of energetic quantities such as internal energy and heat capacity. This is a popular method that has proven its value countless times.

As more computing power became available throughout the years, the number of temperature threads in parallel tempering simulations increased. Large numbers of histograms can cause convergence problems in the recursive reweighting scheme, though. Also, directly estimating other microcanonical quantities that derive from the entropy is more beneficial for a microcanonical statistical analysis [14] than the estimate of the entropy itself.

For this reason, an error-reweighted histogram method without recursion is introduced in the following that also makes use of the same histogram data, but aims at a best-possible, direct estimate for the first derivative of the entropy with respect to energy, i.e., the microcanonical

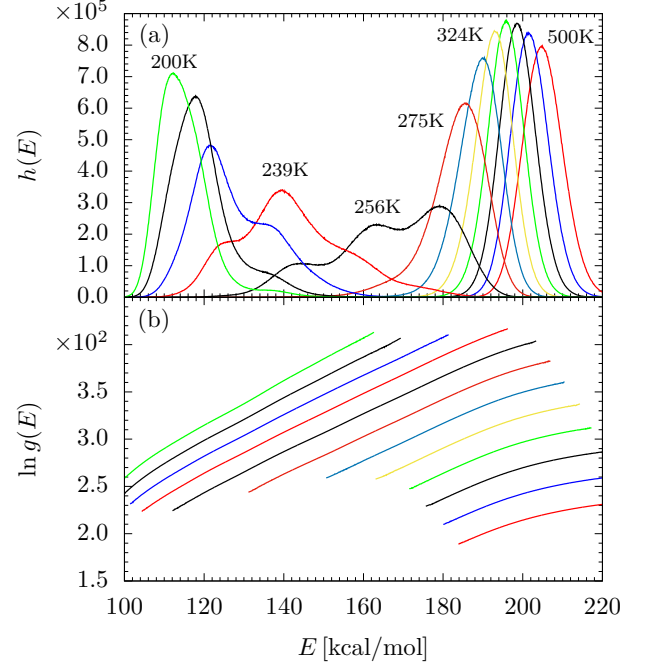


FIG. 1. (a) Raw histograms from parallel tempering simulations of GNNQQNY aggregation in 12 threads with temperatures in the range $T_i^{\text{can}} \in [200\text{K}, 500\text{K}]$, $i = 1, 2, \dots, 12$. A few simulation temperatures are mentioned. (b) Entropy estimators $\ln g(E)$ obtained by naively reweighting the individual histograms.

temperature:

$$\beta(E) = \frac{dS(E)}{dE}. \quad (3)$$

It is important to note that the curvature features of the $\beta(E)$ estimate can already be used for the identification of all transitions the system experiences, independently of their order.

From Eq. (1), we conclude that the i th estimator for the entropy is given by $\hat{S}_i(E) = k_B \ln h_i(E) + E/T_i^{\text{can}} + c_i$, where c_i is constant at T_i^{can} . In the simulations, the energy space needs to be discretized. Assuming a uniform discretization, let ΔE be the energy difference between any two neighboring histogram bins centered at energies E and $E - \Delta E$. Then, the i th estimator for the microcanonical inverse temperature can be written as:

$$\hat{\beta}_i(E) = k_B [\ln h_i(E) - \ln h_i(E - \Delta E)] / \Delta E + 1/T_i^{\text{can}}. \quad (4)$$

Following the similar simple assumption as in the original reweighting approach [27, 28] and in the multicanonical recursion [9, 11] that in the simulations the energy bins are hit sufficiently rarely and that such hits are uncorrelated, the hit frequency follows a Poisson distribution. In this case, the variance of the histogram at the energy E is identical to the average histogram

value, $\sigma_h^2(E) = \langle h \rangle(E)$. Furthermore, it is assumed that $\langle h \rangle(E) \approx h(E)$. This allows us to estimate the error of the logarithm of h from

$$\ln(h \pm \sigma_h) \approx \ln h \pm \frac{1}{\sqrt{h}}. \quad (5)$$

Hence, $\sigma_{\ln h}^2 = 1/h(E)$. As variances of Poisson distributions are additive, the variance for the estimator $\hat{\beta}_i$ in Eq. (4) is

$$\sigma_{\hat{\beta}_i}^2 = \sigma_{\ln h_i}^2(E) + \sigma_{\ln h_i}^2(E - \Delta E) = \frac{h_i(E) + h_i(E - \Delta E)}{h_i(E)h_i(E - \Delta E)}. \quad (6)$$

Using this combined variance as an error weight for the relevance of the i th histogram in the estimation of β from all histograms, we can combine all I estimators $\hat{\beta}_i$ to determine the inverse microcanonical temperature as

$$\beta_{\text{rew}}(E) = \frac{\sum_{i=1}^I w_i(E) \hat{\beta}_i(E)}{\sum_{i=1}^I w_i(E)}, \quad (7)$$

where the error weights are simply $w_i(E) = 1/\sigma_{\hat{\beta}_i}^2$. This is obviously an easy-to-implement result and can in this form already be used for the analysis of microcanonical features that may signal phase transitions. For this purpose, it would be straightforward to extend this approach to derive similarly simple estimators for higher-order derivatives of the entropy, e.g., $\gamma(E) = d^2 S(E)/dE^2 = d\beta(E)/dE$, which can be used to search for inflection points of higher-order transitions. It should also be noted, that the quality of the estimate of $\beta(E)$ allows for the recovery of the entropy $S(E)$ by simple numerical integration. From it the density of states $g(E)$ can be extracted and used for the canonical analysis of energy-dependent averages and response functions such as the heat capacity.

Instead of extending the above method to determine higher-order derivatives of $S(E)$, we follow a different approach here and further improve the estimator (7) by systematically reducing its numerical error by Bézier smoothing [11]. The result is an *analytic function* in E . Hence, calculating the derivatives of the estimate for $\beta(E)$ is straightforward, providing also analytic estimates for the higher-order derivatives of the entropy.

The Bézier method [11, 29, 30] has long been used in computer graphics and design engineering to create smooth curves and surfaces, but it has not yet become a generic tool in systematically improving data quality in scientific applications. Given a discrete set of N points \mathbf{P}_n with $n = 0, 1, \dots, N$, a continuous Bézier curve $\mathbf{B}(t)$, where $t \in [0, 1]$ is the curve parameter, is constructed by

$$\mathbf{B}(t) = \sum_{n=0}^N \mathcal{B}_n^{(N)}(t) \mathbf{P}_n. \quad (8)$$

Here,

$$\mathcal{B}_n^{(N)}(t) = \binom{N}{n} (1-t)^{N-n} t^n \quad (9)$$

are the Bernstein polynomials. Since, for given t , these polynomials are identical to the binomial distribution and therefore already normalized, Eq. (8) can be interpreted as a curve construction method, where each point \mathbf{P}_n contributes to the point $\mathbf{B}(t)$ of the Bézier curve with probability $\mathcal{B}_n^{(N)}(t)$. Alternatively, the position vectors \mathbf{P}_n can be imagined as forces pulling the smooth curve toward their position. It is obvious that this method may be extraordinarily beneficial for the smoothing of numerical data affected by numerical errors (or random noise). If a large number of (ideally) uncorrelated points are scattered around in the vicinity of $\mathbf{B}(t)$, the numerical error at t can be reduced by this robust procedure. If N is sufficiently large, the properties of the Bézier curve do not sensitively depend on it.

In this form, the method works for one-dimensional curves in an embedding space of any dimension. Here, we are only interested in the two-dimensional space, where $\mathbf{P}_n = (E_n, \beta_{\text{rew}}(E_n))$. If n is the index of the histogram bin centered around E_n in discretized energy space, Eq. (8) can simply be rewritten as [11]

$$\beta_{\text{bez}}(E) = \sum_{n=0}^N \binom{N}{n} \left(\frac{E_N - E}{E_N - E_0} \right)^{N-n} \left(\frac{E - E_0}{E_N - E_0} \right)^n \beta_{\text{rew}}(E_n), \quad (10)$$

where the β_{rew} values at the discrete energies E_n obtained by the reweighting method (7) are now used as control points for the generation of the Bézier curve. The range of the discrete energies is $[E_0, E_1, \dots, E_n, \dots, E_N]$, where E_0 and E_N are suitably chosen limits. Since the tails of the histograms close to the lowest and highest simulation temperatures may suffer from insufficient statistics, the boundaries of the energy range could be adjusted, but in effect the impact of those fringes on the results in the most interesting energy regions, e.g., near transition points, is negligible.

Since $\beta_{\text{bez}}(E)$ is an analytic function, derivatives of $\beta_{\text{bez}}(E)$ are easily obtained by differentiating Eq. (10). The result can also be readily implemented; numerical differentiation is not necessary. Higher-order analytic derivatives can be obtained accordingly. The maximum number of analytic derivatives is obviously only limited by the number of data points $\beta_{\text{rew}}(E_n)$ with $n = 0, 1, \dots, N$.

The results of the application of the reweighting method and Bézier smoothing to the GNNQQNY aggregation problem are shown in Fig. 2. The direct estimate of the microcanonical inverse temperature obtained by the reweighting method, $\beta_{\text{rew}}(E)$, is shown as the gray curve in Fig. 2(b). This is a remarkable result. Despite

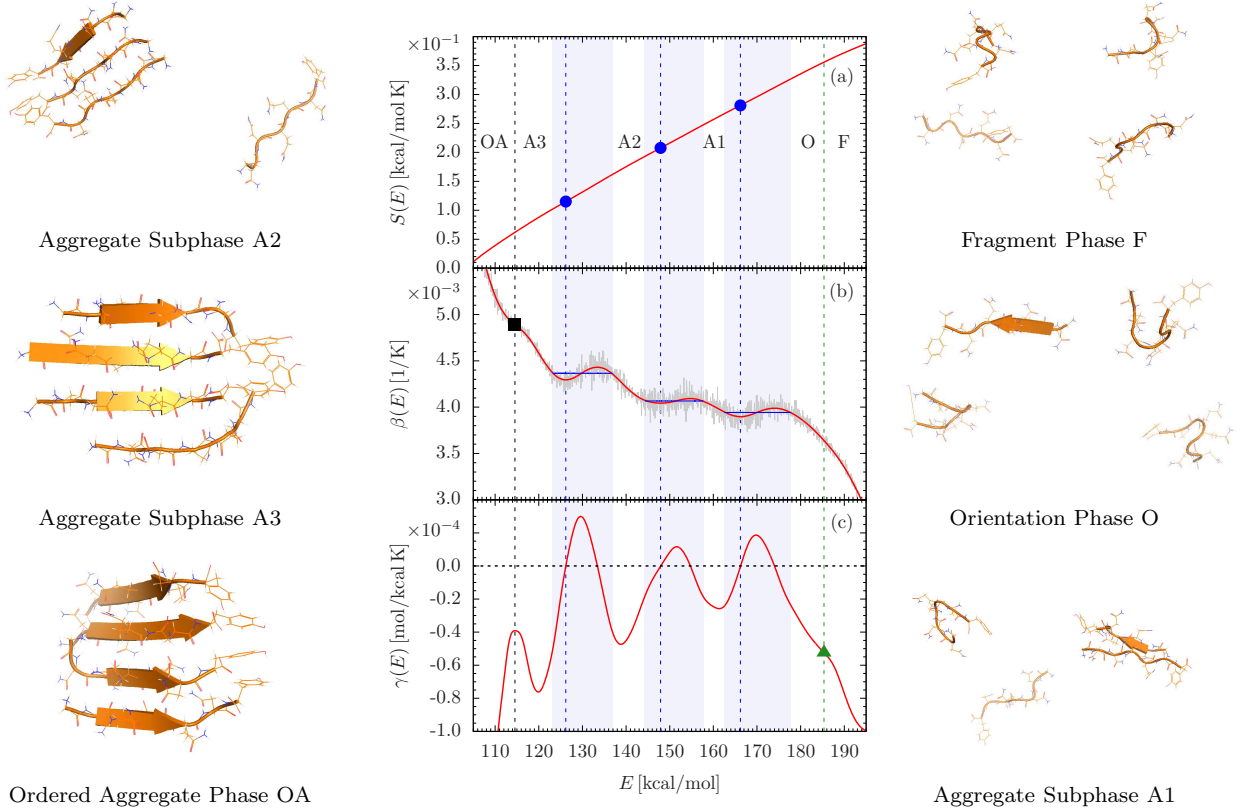


FIG. 2. (a) Microcanonical entropy $S(E)$ of four GNNQQNY chains. (b) Two estimates of the microcanonical inverse temperatures: $\beta_{\text{rew}}(E)$ (grey) obtained by histogram reweighting and the corresponding Bézier curve $\beta_{\text{bez}}(E)$ (red). (c) Second derivative of the entropy $\gamma(E) = d\beta(E)/dE = d^2S(E)/dE^2$ obtained by analytic differentiation of the Bézier curve $\beta_{\text{bez}}(E)$ shown in (b). Circles in (a) and the square in (b) mark least-sensitive inflection points of these curves, indicating independent first- and second-order transitions, respectively. Maxwell constructions for the first-order transitions are shown as horizontal blue lines in (b) and blue shaded areas emphasize coexistence regimes; their widths correspond to the respective latent heats. The triangle in (c) is located at the inflection-point of a dependent third-order transition in the disordered phase. Vertical dashed lines separate the individual phases. Representative conformations in the individual phases are also shown in atomic and cartoon representations. Arrows indicate that values of successive backbone dihedral angles enable the formation of β -strands in those sections of the chain.

the still visible numerical fluctuations, the characteristic backbending features indicating first-order transitions can uniquely be identified. The red curve is the continuous Bézier reconstruction $\beta_{\text{bez}}(E)$ (with $N = 1137$, $E_0 = 103.35$ kcal/mol, and $E_N = 216.95$ kcal/mol) and enhances these features. The derivative of the Bézier curve, $\gamma(E) = d\beta_{\text{bez}}(E)/dE$, is shown in Fig. 2(c). The microcanonical entropy $S(E)$, plotted in Fig. 2(a), is obtained as a byproduct by integrating $\beta_{\text{bez}}(E)$.

The identification and classification of phase transitions and the description of the transition sequence in this system is straightforward with the precise information provided by the generalized microcanonical inflection-point analysis method [14]. Characteristic features of conformations in the energy regions associated with the structural phases such as hydrogen bonds, hydrophobic contacts between side chains, inter-chain contacts, helix and sheet contents, and chain orientations helped reveal

all aspects of the transition sequence. In the fragment phase F, the individual chains are separate and do not exhibit structural features. This changes as the system undergoes a dependent third-order transition into the orientation phase O as indicated by the triangle in $\gamma(E)$ in Fig. 2(c) at about 280 K. This is an important step in the sequence, because individual chains stretch out and even form oriented β -strands, which ultimately enables the inter-chain formation of hydrogen bonds once clusters start forming.

It is worth noting that, in contrast to the typical independent transitions, a dependent transition cannot exist without an independent transition it is associated with. In this case, the corresponding independent transition is the closest first-order transition from O into the aggregate subphase A1, which initiates the aggregation sequence. If present, dependent transitions can only be found in the less ordered phase and therefore serve as a

precursor for the major transition to occur upon reducing energy (or temperature).

Inflection points in $S(E)$ indicate the independent first-order transitions accompanying the aggregation process from A1 (single cluster of two chains) over A2 (one cluster with three chains or two clusters with two chains) to A3 (complete cluster). These are marked by circles in Fig. 2(a). The identification is done best by looking for minima in $\beta(E)$, so $S(E)$ is not even needed for the actual identification of this type of transition. These findings are consistent with results from earlier studies of generic, coarse-grained polymer and protein models [31, 32]. As clusters of chains form, translational entropy is lost, which explains the effective entropic suppression at the corresponding transition energies. Not only do these results confirm the reality of these features, they also emphasize the capability of coarse-grained models to qualitatively reveal these subphase transitions accompanying the overall nucleation transition. If the system would contain more chains, the number of such first-order transitions increases in accordance with the combinatorial number of possible clusters. Eventually, toward the thermodynamic limit, the expectation is that the individual transitions merge into a single first-order nucleation phase transition [32].

This sequence of first-order-like features in nucleation processes is very common and has already been observed in the formation of finite atomic clusters long time ago [33, 34]. Effectively, the cooperative effects of energy and entropy reduction create a barrier in the energy landscape $F(E, T_{\text{agg}}) = -k_B T_{\text{agg}} \ln Z_{\text{res}}(E, T_{\text{agg}})$. The individual histograms recorded at temperatures near the (canonical) aggregation temperature T_{agg} , shown in Fig. 1(a), can serve as estimators of the restricted partition function $Z_{\text{res}}(E, T_{\text{agg}})$. Energy barriers for each nucleation step originate from the respective bimodal shapes of the distributions in those energy regions, where two phases coexist [32].

The aggregate in A3 is mostly stabilized by hydrophobic interaction of the Tyrosine (Y) side chains at the C termini, but at the expense of hydrogen bonds along the strands. Eventually, an independent second-order transition into the ordered aggregate phase OA is found near the lower energy limit in the aggregated phase. The square in Fig. 2(b) marks the corresponding inflection point in the inverse temperature curve and corresponds to the negative peak in $\gamma(E)$, which makes it easy to identify this transition. The transition can be attributed to the proper alignment of the strands by optimizing the number of hydrogen bonds for the formation of a well-organized β -sheet.

To summarize, in this paper a novel microcanonical histogram reweighting method was introduced for the direct estimation of microcanonical quantities such as the microcanonical entropy, inverse temperature, and higher-order derivatives from basic energy histogram data typ-

ically obtained in standard computer simulations. In the context of the previously introduced generalized inflection-point analysis method [14], curvature features of these quantities can then be used for the unique and systematic identification and classification of phase transitions in any physical system of any size. The power of these methods is demonstrated in the application to peptide aggregation. For a system of multiple GNNQQNY heptapeptides, the entire transition sequence ultimately leading to the formation of β -sheet assemblies could be identified. It will be exciting to compare transition hierarchies for different systems in future applications of the method introduced here.

The author thanks the Georgia Advanced Computing Resource Center at the University of Georgia for providing computational resources.

* bachmann@smsyslab.org; <https://www.smsyslab.org>

- [1] R. H. Swendsen and J.-S. Wang, Phys. Rev. Lett. **57**, 2607 (1986).
- [2] K. Hukushima and K. Nemoto, J. Phys. Soc. Jpn. **65**, 1604 (1996).
- [3] K. Hukushima, H. Takayama, and K. Nemoto, Int. J. Mod. Phys. C **7**, 337 (1996).
- [4] C. J. Geyer, in *Computing Science and Statistics*, Proceedings of the 23rd Symposium on the Interface, ed. by E. M. Keramidas (Interface Foundation, Fairfax Station, 1991), p. 156.
- [5] E. Marinari and G. Parisi, Europhys. Lett. **19**, 451 (1992).
- [6] A. P. Lyubartsev, A. A. Martsinovski, S. V. Shevkunov, and P. N. Vorontsov-Velyaminov, J. Chem. Phys. **96**, 1776 (1992).
- [7] B. A. Berg and T. Neuhaus, Phys. Lett. B **267**, 249 (1991).
- [8] B. A. Berg and T. Neuhaus, Phys. Rev. Lett. **68**, 9 (1992).
- [9] B. A. Berg, *Markov Chain Monte Carlo Simulations* (World Scientific, Singapore, 2004).
- [10] W. Janke, Physica A **254**, 164 (1998).
- [11] M. Bachmann, *Thermodynamics and Statistical Mechanics of Macromolecular Systems* (Cambridge University Press, Cambridge, 2014).
- [12] F. Wang and D. P. Landau, Phys. Rev. Lett. **86**, 2050 (2001).
- [13] F. Wang and D. P. Landau, Phys. Rev. E **64**, 056101 (2001).
- [14] K. Qi and M. Bachmann, Phys. Rev. Lett. **120**, 180601 (2018).
- [15] K. Sitarachu and M. Bachmann, Phys. Rev. E **106**, 014134 (2022).
- [16] L. F. Trugilho and L. G. Rizzi, J. Stat. Phys. **186**, 40 (2022).
- [17] G. Pettini, M. Gori, R. Franzosi, C. Clementi, and M. Pettini, Physica A **516**, 376 (2019).
- [18] M. Gori, R. Franzosi, G. Pettini, and M. Pettini, J. Phys. A: Math. Theor. **55** 375002 (2022).
- [19] L. Di Cairano, J. Phys. A: Math. Theor. **55**, 27LT01

- (2022).
- [20] D. Aierken and M. Bachmann, *Phys. Chem. Chem. Phys.* **25**, 30246 (2023).
 - [21] A. Irbäck, B. Samuelsson, F. Sjunnesson, and S. Wallin, *Biophys. J.* **85**, 1466 (2003).
 - [22] A. Irbäck and S. Mohanty, *J. Comput. Chem.* **27**, 1548 (2006).
 - [23] M. Balbirnie, R. Grothe, and D. S. Eisenberg, *Proc. Natl. Acad. Sci. (USA)* **98**, 2375 (2001).
 - [24] J. Gsponer, U. Haberthür, and A. Caflisch, *Proc. Natl. Acad. Sci. (USA)* **100**, 5154 (2003).
 - [25] B. Strodel, C. S. Whittleston, and D. J. Wales, *J. Am. Chem. Soc.* **129**, 16005 (2007).
 - [26] K. L. Osborne, M. Bachmann, and B. Strodel, *Proteins: Struct. Func. Bioinf.*, **81**, 1141 (2013).
 - [27] A. M. Ferrenberg and R. H. Swendsen, *Phys. Rev. Lett.* **63**, 1195 (1989).
 - [28] S. Kumar, D. Bouzida, R. H. Swendsen, P. A. Kollman, and J. M. Rosenberg, *J. Comput. Chem.* **13**, 1011 (1992).
 - [29] P. Bézier, *Automatisme* **13**, 391 (1968).
 - [30] W. J. Gordon and R. F. Riesenfeld, *J. Assoc. Comput. Machin.* **21**, 293 (1974).
 - [31] C. Junghans, M. Bachmann, and W. Janke, *Phys. Rev. Lett.* **97**, 218103 (2006).
 - [32] T. Koci and M. Bachmann, *Phys. Rev. E* **95**, 032502 (2017).
 - [33] R. M. Lynden-Bell and D. J. Wales, *J. Chem. Phys.* **101**, 1460 (1994).
 - [34] D. J. Wales and R. S. Berry, *Phys. Rev. Lett.* **73**, 2875 (1994).